Evidence for a dynamic role for homocitrate during nitrogen fixation: the effect of substitution at the alpha-Lys 426 position in MoFe-protein of Azotobacter vinelandii

Marcus C Durrant, Amanda Francis, David J Lowe, William E Newton, Karl Fisher

Biochemical Journal Immediate Publication. Published on 27 Mar 2006 as manuscript BJ20060102

Evidence for a Dynamic Role for Homocitrate during Nitrogen Fixation: The Effect of Substitution at the α-Lysine426 position in MoFe-Protein of *Azotobacter vinelandii*.

Marcus C. Durrant[†], Amanda Francis, David J. Lowe*, William E. Newton[#] and Karl Fisher*

Department of Biological Chemistry, John Innes Centre, Norwich Research Park, Colney Lane, Norwich NR4 7UH, UK.
[#]Department of Biochemistry, Virginia Polytechnic Institute and State University, Blacksburg, VA 24061, USA
[†]Biomolecular and Biomedical Research Centre, School of Applied Sciences, Ellison Building, Northumbria University, Newcastle upon Tyne, NE1 8ST, UK.

*Authors to whom correspondence should be addressed.
E-mail: karl.fisher@bbsrc.ac.uk and david.lowe@bbsrc.ac.uk

Running title: Dynamic Role for Homocitrate during Nitrogen Fixation
Key words: Nitrogenase, MoFe-Protein, Homocitrate, Nitrogen Fixation

Biochemical Journal Immediate Publication. Published on 27 Mar 2006 as manuscript BJ20060102

ABSTRACT

Although it is generally accepted that the active site of nitrogenase is located on the iron-molybdenum cofactor, the exact site(s) of N_2 binding and reduction remain the subject of continuing debate, with both Mo and Fe atoms being suggested as key players. The current consensus favours binding of acetylene and some other non-biologically relevant substrates to the central Fe atoms of the FeMo cofactor (Dos Santos, P.C., *et al*. (2005) Acc. Chem. Res, 38, 208 – 214). The reduction of N_2 is however a more demanding process than reduction of these alternative substrates because it has a much higher activation energy and does not bind until three electrons have been accumulated on the enzyme. The possible conversion of bidentate to monodentate homocitrate on this three electron-reduced species has been proposed to free up a binding site for N_2 on the Mo atom. One of the features of this hypothesis is that α-lysine426 facilitates chelate ring opening and subsequent orientation of the monodentate homocitrate by forming a specific H-bond to the homocitrate $-CH_2CH_2CO_2^-$ carboxylate group. In support of this concept, we show that substitution of α-lysine426 can selectively perturb N_2 reduction without affecting acetylene reduction. We interpret our experimental observations in the light of a detailed molecular mechanics modelling study of the wild type and altered nitrogenase MoFe-proteins.

Abbreviations used: MoFe-protein, molybdenum-iron protein of nitrogenase, (Av1); FeMo-cofactor, the Fe_7MoS_9X-homocitrate prosthetic group in the MoFe-protein; Fe-protein, iron protein of nitrogenase, (Av2); EDTA, ethylenediamine-tetraacetic acid; EPR, electron paramagnetic resonance; HEPES, *N*-(2-hydroxyethyl)piperazine-*N*'-2-ethanesulfonic acid; MgATP, the magnesium salt of adenosine triphosphate; MM, molecular mechanics; NMF, N-methyl formamide; SDS-PAGE, sodium dodecyl sulfate polyacrylamide gel electrophoresis; CE, crude extract; SPA, specific activity. Altered nitrogenase MoFe-proteins are designated by the name of the subunit, either α or β, followed by the three-letter code for the substituting amino acid and the number of the amino-acid position substituted.

Biochemical Journal Immediate Publication. Published on 27 Mar 2006 as manuscript BJ20060102

INTRODUCTION

Nitrogenase is the complex metal-containing enzyme responsible for the conversion of atmospheric N_2 into NH_3. The most extensively studied nitrogenase, Mo-nitrogenase, contains Mo and Fe and consists of two separable proteins known as the MoFe and Fe-proteins [1]. The MoFe-protein is an $\alpha_2\beta_2$ tetramer that contains two copies each of a pair of highly distinctive metal-sulfur clusters known as the P-cluster and FeMo-cofactor (FeMoco); these are implicated in electron transfer and substrate reduction, respectively. The second enzyme component, the Fe-protein, contains an Fe_4S_4 cluster and two MgATP-binding and -hydrolysis sites; it is the obligate electron donor to the MoFe-protein. FeMoco is an inorganic cluster formulated as $MoFe_7S_9X$, where X is a light atom at the centre of the cluster, plus an organic ligand identified as (*R*)-homocitrate [2-3], which is attached to the Mo atom giving a five-membered chelate ring. The cofactor binds within the MoFe-protein α-subunit and is covalently attached to the protein *via* α-Cys275 and α-His442, which bind to the terminal Fe and Mo atoms respectively (see Figure 1). The inorganic part of the FeMoco is tightly packed within the MoFe-protein and surrounded by (i) residues that approach each of its three faces (α-Val70, α-Arg359 and α-Phe381), (ii) residues that have the potential to H-bond to the bridging sulfide atoms (α-Arg96, α-His195, α-Gly356 and α-Gly357), and (iii) a residue that has the potential to H-bond to an S atom contained within the $MoFe_3S_3$ sub-cluster fragment (α-Arg359) [4].

N_2 reduction by wild-type Mo-nitrogenase requires an anoxic environment, an adequate supply of MgATP and a reductant of sufficiently low potential. Both component proteins are absolutely required for enzymatic activity. A detailed scheme consisting of three main phases has been developed to describe the kinetics of the interactions between the two nitrogenase component proteins [5]. First the MoFe-protein associates with the one-electron-reduced Fe-protein that has two molecules of MgATP bound, then an electron is transferred from the Fe-protein to the MoFe-protein and both molecules of MgATP are hydrolyzed, and finally the two proteins dissociate, allowing re-reduction (typically by dithionite *in vitro* and ferredoxin/flavodoxin *in vivo*) of the Fe-protein and replacement of the MgADP

by MgATP. For N_2 to be reduced to NH_3, a minimum of eight of these cycles must take place. The rate at which electrons appear in the product is independent of the substrate being reduced because the rate-determining step in turnover is the dissociation of the Fe-protein from the MoFe-protein. This situation leads, under ideal conditions, to a constant ratio of the rate of MgATP hydrolysis to the rate of transfer of electron pairs to product (the ATP:$2e^-$ ratio) of 4:1.

A number of resting-state structures of both nitrogenase component proteins, both separately and as complexes, have been solved by X-ray crystallography [6-9]. However, these structures have given relatively little information about how N_2 and alternative substrates interact with the active site because wild type nitrogenase only binds substrates under conditions of enzymatic turnover [1]. The debate continues as to whether N_2 binds to Fe or Mo at the active site although evidence is accumulating that alternative substrates, such as C_2H_2 and propargyl alcohol, bind initially to one or more Fe atoms [10].

Recent spectroscopic studies have detected species derived from hydrazine and methyl diazine; these are both substrates of altered proteins and are a potential intermediate and intermediate analogue respectively,, in N_2 reduction [11]. Even more significantly, an enzymic state derived from N_2 itself has been observed for the wild-type protein [12] albeit under conditions, with an excess of MoFe-protein over Fe-protein, where N_2 is not reduced and does not inhibit proton reduction. These studies were interpreted as supporting the hypothesis that the binding site of these nitrogenous species is on the same α-Val70 Fe-S face of FeMoco as that assumed to bind alkynes, because the binding of hydrazine and methyldiazene is affected by mutations close to this face [11].

In the absence of any direct experimental evidence for the mode of N_2 binding and reduction, a variety of theoretical models has been developed using quantum calculations[13-17]. Although a consensus has not yet been reached from these studies, they do at least illustrate the various possibilities. A model assuming that the structure of the FeMo-cofactor remains unchanged during N_2 reduction has been explored in greatest detail by Dance[16-17]; it suggests that the Mo atom remains six-coordinate throughout

the catalytic cycle and N_2 reduction proceeds entirely on the Fe atoms of the cluster. Alternative models allow the structure of the FeMoco to be more dynamic during turnover, with one or more of its bonds undergoing temporary cleavage to open up coordination sites for N_2 (see Scheme 1). Blochl *et al*. have developed one such model based on cleavage of an Fe-S bond in the core cluster [14]. The N_2 ligand then bridges between Fe atoms prior to reduction and again the Mo/homocitrate moiety plays no active role in catalysis.

These models may be thought of as being compatible with the existence of two alternative nitrogenases. The better established of these is V-nitrogenase in which V takes the place of Mo, whereas the third is more poorly characterized but appears to contain only Fe. Although Mo and V have similar chemistries, associated with their diagonal relationship in the Periodic Table, Fe is clearly different. Because all three nitrogenases reduce N_2, it has been inferred that the heterometal, the Mo/homocitrate part of the FeMoco, is not directly involved and only provides 'fine tuning'. However, all three nitrogenases contain homocitrate and changes to the homocitrate ligand, such as its replacement by citrate in the *ΔnifV* MoFe-protein [19-20], drastically impair their ability to reduce N_2 [21]. The importance of homocitrate for N_2 reduction raises the possibility that the Mo site, or its equivalent in the alternative nitrogenases, is directly involved by cleavage of one of the bonds to homocitrate upon reduction of the enzyme [22-25]. Support for this hypothesis comes from two sources. First, studies with model complexes have shown that protonation of a carboxylate ligand upon reduction of a Mo complex can indeed open a chelate ring and result in subsequent binding of N_2 [22]. Second, experiments performed on extracts of isolated FeMoco showed a specific interaction between homocitrate and an imidazole ligand on Mo, which were interpreted in terms of a cluster-activating interaction between monodentate homocitrate and the protein ligand of Mo, α-His442 [23]. Further, critical dependence on Mo was shown by Hales and co-workers, who succeeded in substituting W for Mo in the FeMo-cofactor and showed that the modified enzyme was unable to reduce N_2 [26].

Biochemical Journal Immediate Publication. Published on 27 Mar 2006 as manuscript BJ20060102

An important feature of the homocitrate ring-opening model is that it includes an experimentally testable feature, namely a specific role for α-Lys426 in N_2 reduction but not in C_2H_2 reduction. Thus, C_2H_2 reduction can proceed on the central Fe sites of FeMoco, using states of the MoFe-protein that are not sufficiently reduced to induce homocitrate ring opening, whereas the reduction of N_2 requires the more reduced MoFe-protein states that can undergo ring opening. The α-Lys426 side chain then acts to orientate the monodentate homocitrate ligand in two ways. First, a general electrostatic interaction between the cationic Lys side chain and the anionic $-CH_2CH_2CO_2^-$ arm of homocitrate helps to rotate the monodentate homocitrate away from the Mo and into the correct position to allow N_2 binding at Mo. Secondly, a specific H-bond between these two groups orientates the homocitrate $-CH_2CH_2CO_2^-$ arm in such a way that an additional H-bond is formed between the latter group and the -NH group of α-His442. Although probably quite weak in energy terms, this interaction could provide a valuable enhancement of the reactivity of the Mo site with respect to initial reduction of N_2. Similar effects would operate in the alternative nitrogenases, but not in the Δ*nifV* mutants.

In this paper, we show that substitutions at the α-Lys426 position can impair the enzyme's ability to reduce N_2 without affecting its C_2H_2-reducing characteristics. We interpret the details of our observations in terms of the homocitrate ring-opening hypothesis by means of molecular mechanics calculations, and provide further evidence that the protein environment is tailored for homocitrate ring opening by analysis of the available amino acid sequences for Mo and V nitrogenases.

EXPERIMENTAL

Microorganisms and site-directed mutagenesis.

The wild type bacterium used throughout this study was strain DJ527, an *Azotobacter vinelandii* strain containing an insertion mutation within *hoxKG*, which knocks out uptake hydrogenase activity but retains the *nif* genes intact.

Mutant strains. Site-specific changes were made using overlap extension PCR methodology (SOE) [27]. Mutations generated by SOE-PCR were transformed into *A. vinelandii* deletion strain DJ100 and selected on the basis of restored Nif^+ phenotype prior to sequencing to confirm the presence of the desired change.

***A. vinelandii* cell growth and nitrogenase expression.**

The growth of wild type and altered *A. vinelandii* strains was as reported by Shen *et al* [28]. Culture density was monitored using a Klett-Summerson meter (Klett Mfg. Co. Inc., NY, USA) equipped with a no. 54 filter. Ideally, a mid-log culture with a Klett of 100-150 units was used to inoculate a 28-L fermentor. Cultures were grown overnight in 24 L of a fixed nitrogen-rich basal liquid Burk medium [29] in the 28-L fermentor (New Brunswick Scientific Co., New Brunswick, NJ, USA) with a dissolved O_2 concentration of 25% maintained by varying the flow of compressed air, N_2 gas, and the stirring rate.

Nitrogenase expression was induced at a cell density of 250 Klett units by centrifuging cells at 8,000 x g at 30ºC and resuspending in 24 L of a fixed nitrogen-free medium made from deionized water containing 10 μM Na_2MoO_4, 20 μM $FeCl_3$ and Burks sucrose basal media in the fermentor. The dissolved oxygen concentration was maintained at 25% for three and a half hours before harvesting.

Crude-extract preparation and nitrogenase protein purification.

Whole cell rupture was accomplished by osmotic shock as follows. Approximately 200 g of cells were thawed under an N_2 atmosphere and then diluted with 750mL anaerobic 25 mM Tris-HCl (pH 8.0), containing 4 M glycerol and 2 mM sodium dithionite. After resuspension, the cells were spun at 14,000 x g and 4ºC for 30 minutes. The supernatant was discarded and the cell pellets were resuspended in approximately 400 mL 25 mM Tris pH8 containing a small amount of DNase. After violent shaking under an N_2 atmosphere, the extract was transferred anaerobically into 95-mL ultracentrifuge tubes and centrifuged at 4°C for 90 min at 98,000 x g.

Unless otherwise stated, the buffer system used throughout protein purification was 25 mM Tris-HCl, pH 7.4, containing 2 mM sodium dithionite.

The purification of the nitrogenase MoFe-protein involved Q-Sepharose and anion-exchange chromatography, Sephacryl S-200 gel filtration and lastly phenyl Sepharose hydrophobic-interaction chromatography exactly as described by Kim *et al* [30].

The Fe-protein was purified to homogeneity *via* fractionation from a second Q-Sepharose anion-exchange column.

All chromatography columns were run at room temperature and were made anaerobic before use by flushing with dithionite-containing anaerobic buffer until the eluant was able to reduce methyl viologen. The elution profile of the proteins was monitored at 365 nm with an in-line Pharmacia LKB Uvicord SII absorbance detector cell (Amersham Biosciences, Sweden) coupled with a single-channel chart recorder. Coloured fractions were collected anaerobically in N_2-flushed conical flasks.

Purified nitrogenase proteins were concentrated separately in an Amicon micro-filtration apparatus using either a 30K or 100K MWCO membrane before buffer exchange into 25 mM HEPES, 10 mM $MgCl_2$, 200 mM NaCl, pH 7.4 by passage through an anaerobic P-6DG (BioRad, Hemel Hempstead, UK) column in an anaerobic glove box with an O_2 concentration of less than 1 ppm.

Assay of nitrogenase activity.

Nitrogenase-catalyzed C_2H_2 reduction (10% C_2H_2/90% Ar), N_2 reduction (100% N_2) and proton reduction (100% Ar) were assayed in 7.8-mL reaction glass serum vials fitted with No 25 suba seal rubber stoppers as previously described [30]. Stock 100% C_2H_2 was generated from the reaction of calcium carbide (BDH, Poole, UK) with water and subsequently diluted to 10% in the assay. *A. vinelandii* Fe-protein used in this study had a specific activity of 3000 nmol H_2 (min.mg protein)$^{-1}$, the MoFe-protein specific activities are listed in Table 1.

The apparent K_m for C_2H_2 reduction catalyzed by Av1 was determined by entering the C_2H_2-reduction rate as a function of C_2H_2 concentration into SigmaPlot 8.0. Steady-state assays containing 0.2-0.001 atm C_2H_2 were

performed under maximal flux conditions (Fe-protein:MoFe-protein ratio of 20:1).

Product analysis.

Product formation was measured by gas chromatography using a GC-14B Gas Chromatograph with a Shimadzu Class-VP Chromatography Automated Data Software System (Shimadzu, Tokyo, Japan). C_2H_4 was quantified on a Poropak N column using a flame-ionization detector. H_2 evolution was also measured by gas chromatography with a molecular sieve 5Å column and a thermal conductivity detector. Both systems were calibrated by injection of standard gases.

NH_3 production was measured by phenol/hypochlorite colorimetry [26, 28]. MgATP hydrolysis was determined as described by Dilworth *et al*. [31-32].

Protein estimation, metal estimation, EPR measurements and SDS-PAGE.

Nitrogenase-protein concentrations were estimated by the Lowry method [33] with bovine serum albumin as a standard. Absorbances were read, after colour development, at 750 nm in 1-cm path length cells. Both the Mo and Fe contents of the purified nitrogenase proteins were determined by inductively coupled plasma atomic emission spectroscopy using a Perkin-Elmer Plasma 400 spectrometer (Norwalk, CT, USA). The EPR spectra of the purified MoFe-proteins were recorded at X-band on a Bruker ELEXYS 500 instrument with an ER094X microwave bridge and an ER4122SHQ cavity [34]. Sodium dodecyl sulfate-polyacrylamide electrophoresis (SDS-PAGE) was employed to check nitrogenase expression in crude extracts and to estimate the purity of the MoFe and Fe-proteins after each column chromatography step. Samples and gels were prepared according to the method of Laemmli [35]. Running gels were 10% polyacrylamide with 1.35% cross-linker and stacking gels were 4% polyacrylamide. Electrophoresis was carried out at 25 mA, using a mini-Protean 3 electrophoresis apparatus (BioRad, Hemel Hempstead, UK) and 10 – 250kD Kaleidoscope pre-stained molecular weight markers (BioRad, Hemel Hempstead, UK).

Molecular modelling.

Molecular modelling studies were performed using Insight II [36]. The 1.16 Å X-ray crystal structure of nitrogenase [3], Protein Data Bank [37] accession code 1MIN was edited to a working model consisting of one FeMoco plus all of protein chains α and β, residues 350-523 of chain β', and 19 water molecules defining the 'water pool' around homocitrate (chains labelled as A, B and D respectively in 1MIN). Partial atomic charges for the FeMoco were assigned based on the results of density functional theory calculations [16, 18], and the central atom assumed to be N. H-atom positions and partial atomic charges for the protein and water were calculated at pH 7.0, using the charged capping mode. The waters were aligned manually so as to maximize H-bonding with the surrounding protein. Energy minimizations on the resting-state structures were carried out using the consistent valence force field and steepest descent algorithm within the Discover module of Insight II, with the following groups kept fixed: Mo, Fe, S and N atoms of FeMoco; ND1 atom of α-His442; O5 and O7 of homocitrate; α-chain residues 4-55 (all atoms), 56-71 (backbone), 72-93 (all atoms), 94-98 (backbone), 99-189 (all atoms), 190-192 (backbone), 193-352 (all atoms), 353-360 (backbone), 361-378 (all atoms), 379-382 (backbone), 383-415 (all atoms), 416-420 (backbone), 431-446 (backbone), 447-480 (all atoms); β-chain residues 2-94 (all atoms), 95-106 (backbone), 107-523 (all atoms); β'-chain residues 350-523 (all atoms). For the ring-opened structures, water number 154 was replaced with an N_2 ligand attached to the Mo, the initial monodentate homocitrate geometry was constructed according to our earlier model [22], and additional fixed atom restraints were included as follows; N_2 ligand, all of α-His442, and O4 of homocitrate; O3 was allowed to relax. Values for the distance-dependent dielectric constant of 10.0 and the Coulombic scale factor of 2.0 were chosen empirically by comparing the results of trial geometry optimizations with the original crystal structure; these values were found to reproduce the original structure to within satisfactory limits. The RMS deviation for superimposition of all the heavy protein atoms in the optimized geometry with the crystal structure was 0.046 Å, although a few side chains had relatively large atomic movements (up to 1 Å) due to rotations, and some of the water molecules in

the water pool had moved by up to 0.6 Å. For each mutant as well as the wild type structure, geometry optimizations were carried out as above, on both the homocitrate-closed and homocitrate-open conformations. Where the side chain of the substituting residue was significantly smaller than the wild type α-Lys426 residue, one or two extra water molecules were included in the model.

RESULTS

General physical and catalytic properties

Eleven mutant strains, each having a specific amino-acid substitution at the α-426 position in the MoFe-protein of *A. vinelandii,* were constructed and their proteins expressed and purified. Table 1 summarizes the MoFe-protein proton-reduction specific activities for crude extracts and MoFe-proteins purified from nitrogenase-depressed wild-type and mutant strains, together with their diazotrophic growth behaviour. All eleven α-426 mutant strains are capable of diazotrophic growth, although they all show impaired growth rates under diazotrophic conditions in fixed-nitrogen-free medium compared to the wild type strain. Four of them, which carry the altered MoFe-protein with substitution to Ala, Gln, Thr or Ser at this position, fix N_2 almost as efficiently as wild type with doubling times of about 4 - 4.5 hours. The doubling times for growth on N_2 for the other strains range from 5 - 6 hr for the Arg-, His-, and Met-substituted strains through 8 - 13 hr for the Tyr-, Glu-, Asp-, and Trp-containing strains.

All mutant strain crude extracts showed similar Fe-protein specific activities, indicating that nitrogenase was derepressed effectively during cell growth (data not shown). However, the crude extract H_2-evolution activities under Ar are all lower than the wild-type activity, which suggests that FeMoco insertion into the MoFe-proteins has been compromised.

After purification, only the α-Arg426 and α-Gln426 MoFe-proteins contain a Mo complement and H_2-evolution specific activity similar to wild type MoFe-protein. The α-Ser426, α-Thr426 and α-Ala426 MoFe-proteins contain 50% or more of the expected Mo content, whereas the other altered proteins range from 40 to 10% of the possible maximum. In all cases, the lowered metal content is consistent with their lowered H_2-evolution activity and S=3/2

EPR-signal intensity. No new dithionite-reduced resting-state EPR features were observed from any of the purified altered MoFe-proteins.

Although each altered MoFe-protein was purified using exactly the same procedure as that employed for the wild type MoFe-protein, different levels of purity were achieved as shown by SDS-PAGE (Figure 2). The α-Gln426, α-Thr426 and α-Arg426 MoFe-proteins were of comparable purity to the wild type MoFe-protein, whereas the others contained either high or low molecular-weight contaminants or both. In addition, the α-Glu426, α-Trp426 and α-Tyr426 MoFe-proteins do not contain equal amounts of the α- and β-subunits, which is consistent with the lowered Mo content of these proteins.

With one exception, the addition of 10% CO to nitrogenase assays, under conditions of high electron flux, resulted in the complete inhibition of C_2H_2 reduction with all electrons being directed to hydrogen formation (data not shown). However, the α-426Arg MoFe-protein, when complemented with a large excess of wild-type Fe-protein, has H_2-evolution activity that is inhibited by CO. CO maximally inhibits the activity by 50%, which is comparable to that previously observed for the Δ*nifV* and α-Lys191 altered MoFe-proteins [38]. Because the rate of MgATP hydrolysis is not similarly inhibited by CO, the ATP:$2e^-$ ratio increases by 2 - 3-fold for this MoFe-protein in the presence of CO. The K_I for CO inhibition of H_2 evolution for the α-426Arg MoFe-protein was measured as 5.5 x 10^{-3} kPa, which is comparable to the values of 8 x 10^{-3} kPa and 4 x 10^{-3} kPa measured previously for the α-Lys191 and *ΔnifV* MoFe-proteins, respectively [38]. These values, although similar, appear directly to reflect the extent of the inhibition by CO**.**

EPR spectra obtained by freeze quenching during turnover in the presence of CO were identical to those observed with the wild type and the Δ*nifV* MoFe-proteins [38].

The effect of substituting at the α-426 position on both C_2H_2 and N_2 reduction by purified MoFe-protein.

Table 2 shows that when the α-426 altered MoFe-proteins were assayed under a 10% C_2H_2/90% Ar atmosphere under high electron-flux conditions, the primary product was C_2H_4. Only the α-Asp426 and α-Trp426 MoFe-

proteins produced a significantly higher percentage of H_2 than the wild type enzyme. None of the proteins were capable of reducing C_2H_2 through to C_2H_6, a phenotype of the Δ*nifV* protein. For the wild type (α-Lys426) MoFe-protein assayed under maximal flux conditions, a K_m of 0.83 kPa C_2H_2 was calculated; this falls within the range reported previously [28, 38]. Similar binding affinities were calculated for the altered MoFe-proteins with values between 0.31 and 0.9 kPa. Surprisingly, the highest and lowest apparent binding affinities were obtained for the α-Asp426 MoFe-protein, which showed the lowest percentage of electrons to C_2H_4, and the α-Arg426 MoFe-protein that was our most conservative substitution, respectively.

The addition of 5% or higher C_2H_2 resulted in a 70% inhibition of electron flux through the α-Asp426 MoFe-protein without affecting the rate of ATP hydrolysis. This resulted in an increase in the ATP:2e ratio from approximately 8 while reducing protons to more than 35 in the presence of saturating C_2H_2. The percentage of the total electrons that were diverted to H_2 remained constant in the presence of saturating C_2H_2. Inhibition of nitrogenase turnover by C_2H_2 was not observed with any other MoFe-protein used in this study. Because C_2H_2 acted as an inhibitor of total electron flux, it was only possible to estimate the K_m for C_2H_2 reduction from low, <5kPa, C_2H_2 concentrations.

Neither the rate of complex dissociation nor the rate or amplitude of primary electron transfer from Av2 to the MoFe-protein were affected by the presence of C_2H_2 (data not shown).

When assayed under 100% N_2, the percentage of total electrons transferred to NH_3 varied from 74% for the α-Gln426 MoFe-protein to 35% for the α-Trp426 MoFe-protein (Table 2). The α-Gln426 MoFe-protein was reproducibly better at fixing N_2 than the wild type enzyme, whereas the *ΔNifV* MoFe-protein was more compromised with respect to N_2 reduction than any of the 426-altered MoFe-proteins. Only the Tyr-, Glu-, Asp- and Trp-substituted MoFe-proteins exhibited electron transfer that was uncoupled from MgATP hydrolysis, a phenomenon mirrored in the presence of C_2H_2 and possibly arising from the presence of apo-MoFe-protein in the enzyme preparations. By measuring the NH_3 formed at various N_2 concentrations we were able to determine the K_m for N_2 binding to the wild type MoFe-protein as 8.2 kPa, in

agreement with literature values. The altered MoFe-proteins gave similar K_m values, apart from the α-Arg426 MoFe-protein, which had a K_m approximately three-fold higher; this reduced binding affinity was accompanied by a decreased electron allocation to NH_3 but not an uncoupled ATP:2e ratio.

The effect of substituting at the α-Lys426 position is clearly shown by a plot of percentage electrons consumed by C_2H_4 production against those producing NH_3 (Figure 3). The linear correlation strongly implies that N_2 reduction, but not C_2H_2 reduction, is compromised in these altered proteins. The only exceptions are the α-Asp426 and α-Trp426 altered MoFe-proteins, which also show a significant effect on N_2 reduction. Furthermore, the α-Arg426 altered protein is a surprisingly poor N_2 reducer for such a conservative alteration.

Molecular Modelling

Each altered protein was modelled in two forms, namely the 'closed' form in which the homocitrate chelates the Mo atom as seen in the X-ray crystal structures, and an 'open' form in which the Mo-O bond to the homocitrate β-carboxylate group has broken and the homocitrate has rotated to allow coordination of N_2 at the Mo. Amino-acid substitutions were introduced such that, as far as possible, the positioning of the new side chain followed that of the original. The number of waters in the homocitrate water pool was adjusted to reflect the size of the α-426 mutant side chains; α-Ala426 gained two extra waters, α-Arg426, α-Trp426 and α-Tyr426 each lost one water, and the rest were unchanged. Geometry optimizations of both closed and open forms were carried out using consistent procedures for each protein.

Considering the closed forms first, the only significant displacements of the protein backbone were seen for the α-Trp426 and α-Tyr426 altered proteins, where accommodation of these bulky side chains necessitated significant perturbations of the protein backbone (Cα-426 displacements compared to the wild type of 0.82 and 0.86 Å, respectively). In the case of the α-Trp426 protein, the β-Ser101 side chain rotated through *ca.* 110˚ during the geometry optimization, in order to relieve close contacts with the Trp side chain. These steric clashes have significant consequences for the H-bond normally seen between O3 of the homocitrate $-CH_2CH_2CO_2^-$ arm and the

backbone NH of α-Ile425 in the resting state structure. In the wild type structure, this interaction is characterised by an O··N distance of 2.84 Å in the X-ray crystal structure and 2.89 Å in the geometry optimised structure. It is lost in the closed forms of both the α-Trp426 and α-Tyr426 altered proteins, which show O··N distances of 4.53 and 3.52 Å, respectively; for the α-Trp426 protein, a significant movement of the homocitrate $-CH_2CH_2CO_2^-$ arm means that O4, rather than O3, of homocitrate is now weakly H-bonded to the NH group (O··N distance 3.42 Å). The α-Tyr426 protein shows another interesting feature in that an H-bond has developed between the Tyr OH group and the homocitrate $-CH_2CH_2CO_2^-$ arm (O···O distance 3.35 Å, Figure 4) with the homocitrate moving towards the Tyr to facilitate this bond formation (homocitrate O atom is displaced by 0.83 Å). The closed forms of the other variants all show essentially unperturbed homocitrate geometries, with preservation of the H-bond between homocitrate and α-Ile425 (O··N distances of 2.92 – 2.99 Å). Besides α-Tyr426, only one other altered protein shows a direct interaction between the new side chain and homocitrate; the α-Arg426 protein shows a strong, bifurcated H-bond with O4 of the homocitrate $-CH_2CH_2CO_2^-$ arm (O···N distances 2.87 and 2.99 Å, Figure 5) in addition to the normal H-bond between O3 and α-Ile425. Finally, neither the Glu nor Asp altered proteins show any perturbation of the homocitrate; however the Asp variant is noteworthy in that the side chain is orientated towards β-Arg100 in the neighbouring subunit (Figure 6). The closest contact between these two residues in our model is 3.12 Å, between the carboxylate O and the Arg Nδ. Although the orientation of this interaction does not permit an explicit H-bond, this would probably be possible given greater flexibility for the β-chain than allowed for in our modelling procedure, which kept all the backbone atoms of the β-chain fixed. The extra CH_2 group in the Glu mutant, compared to Asp, appears to weaken the interaction with β-Arg100 and orientate the α-Glu426 back towards homocitrate (Figure 7).

Turning to the ring-opened models, our modelling strategy was determined by two considerations. First, in the wild type enzyme, we postulate that the α-Lys426 side chain promotes homocitrate ring opening through a general electrostatic effect. Second, the side chain promotes the specific orientation of the homocitrate $-CH_2CH_2CO_2^-$ arm required for

activation of FeMoco by interaction with α-His442. We therefore built the α-His442-homocitrate interaction into our models by keeping the position of homocitrate O4 fixed; the rest of the homocitrate was allowed to move. The optimised structures should then give an indication of whether the α-His442-homocitrate interaction is accessible or not. The results fall into several different categories. First, the Ala, His, Met and Thr side chains show essentially no interaction with homocitrate (Ser was not modelled because it is so similar to Thr); of these, the Met side chain approaches closest, to within Van der Waals contact (O···CH_3 distance 3.60 Å). This suggests that these residues would neither hinder nor enhance the interaction between homocitrate and α-His442. The large Trp and Tyr side chains are in contact with the homocitrate -$CH_2CH_2CO_2^-$ arm, suggesting that these groups will sterically hinder realisation of the correct homocitrate geometry. The Arg mutant side chain also contacts the homocitrate -$CH_2CH_2CO_2^-$ arm in its open conformation, with a favourable electrostatic interaction in this case (O···N distance 3.19 Å), but the geometry prevents formation of a specific H-bond. Neither of the two acidic residues, Glu and Asp, has very close contacts with homocitrate, though Glu has the closest approach (O···O distances of 4.13 and 4.25 Å for Glu and Asp respectively). Finally, Gln is the only other residue, apart from the wild type Lys, that forms a specific H-bond with O3 of homocitrate in the ring-opened conformation (Figure 8); both hydrogens of the side chain NH_2 group are involved in a bifurcated H-bond (O···N distance 3.03 Å; O···H distances 2.66 and 2.79 Å). In all cases, homocitrate retains its H-bond to α-Gln191 in both the ring-closed and -open conformations.

Sequence comparisons and homology modelling

In order to investigate the level of conservation of α-Lys426 in known nitrogenase sequences, we searched the Uniprot database for nitrogenase component 1 α-chain proteins, using the *Klebsiella pneumoniae* sequence as a query. Sequences returned by this search were discarded if they were significantly incomplete or if they lacked any of the four Cys and one His residues required for FeMoco and P-cluster binding. The remaining sequences were screened for redundancy and gene annotation, giving 68 α-chain MoFe-protein (NifD) and six α-chain VFe-protein (VnfD) sequences.

These were aligned using the MUSCLE server [40]. This showed that α-Lys426 is strictly conserved across all 68 NifD sequences. Interestingly, however, the equivalent residue in all of the VnfD sequences is Arg. Another significant difference is seen in the preceding residue, α-Ile425 in Av1; in the NifD sequences, this is Ile (50 sequences), Val (17 sequences), or Leu (one sequence), but Pro in all six VnfD sequences. The sequence variations in the vicinity of α-Lys426 are summarised in Table 3.

DISCUSSION

Certain amino acid residues in FeMoco's environment within the MoFe-protein influence its orientation and/or its catalytic and electronic properties as shown by targeted substitution ([10] and references therein). Most of the published data focuses on the interaction of inhibitors, such as CO or the substrate C_2H_2 with altered nitrogenase proteins. For example, all substitutions at the α-Gln191 position exhibit CO-sensitive H_2 evolution and reduce C_2H_2 poorly with C_2H_6 as a product [41]. In this study, we have pinpointed a residue, α-Lys426, which we believe could act to position homocitrate such that N_2 reduction is optimized. In addition to the functional role of this residue during nitrogenase turnover, our experimental results suggest a structural role in terms of insertion of the FeMoco into the apoprotein. Thus, several of our altered proteins contain low or very low levels of functional FeMoco, evidenced by their low EPR intensities, poor catalytic abilities and low Mo contents. The importance of αLys426 in helping to orient FeMoco during its insertion into the MoFe-protein has been inferred by comparison of the fully complemented and FeMoco-free protein crystal structures [42]. The ease of FeMoco insertion into the apoprotein correlates reasonably well with the expected steric and electrostatic properties of the α-426 residue. Thus, the two basic residues, Lys and Arg, have full FeMoco complements, whereas the Gln residue, which also appears to have the potential to form an H-bond to homocitrate (see above), has the next best. The unfavourable electrostatic properties of the two acidic residues, Glu and Asp, and the steric problems associated with the very bulky residues Trp and Tyr, explain why these four mutants have very low FeMoco complements. The other residues have intermediate FeMoco complements. The only inconsistency found is for His, which has an

unexpectedly poor FeMoco complement; we speculate that this is due to some specific but undetermined effect, perhaps arising from this residue's ability to act as a ligand in its own right. Although the proteins have a wide range of activities, the good correlation between EPR intensity and specific activity for H_2 reduction supports the assumption that only properly assembled nitrogenase molecules are catalytically active for the reduction of H_2, N_2 and C_2H_2 in our preparations.

Our experimental data for the α-426 mutants are broadly consistent with the premise that a mutation that perturbs the homocitrate ring-opened state should selectively affect N_2 reduction but not C_2H_2 reduction. Thus in general, the altered proteins have a much wider range of N_2-reduction efficiencies than C_2H_2-reduction efficiencies. The efficiencies of the mutants for N_2 reduction span a range between that of the wild type protein and the Δ*nifV* mutant; this result was expected, because replacement of homocitrate by citrate in the Δ*nifV* mutant is a direct change to the FeMoco structure and should have a greater effect than the more distant perturbations from our substitutions.

There are two exceptions to the general trend, namely Trp and Asp. The Trp variant scores poorly against every measure of its activity, including C_2H_2 reduction, and this is readily explained by the perturbations in the protein structure required to accommodate this very bulky residue. The Asp mutant is more interesting because it alone shows reasonable N_2-reduction activity but poor C_2H_2-reduction activity. Our modelling studies suggest that this anomalous behaviour is not due to some specific interaction between α-Asp426 and homocitrate, but to an interaction between α-Asp426 and β-Arg100 which lies in an α-helix containing one of the P-cluster ligands, β-Cys95; it seems reasonable to suppose that a specific H-bonding interaction between these two residues could distort the structure of the protein. Why this should perturb C_2H_2 reduction so dramatically but hardly affect N_2 reduction is not clear. Although other point mutations that inhibit C_2H_2 but not N_2 reduction are known [43], there are none that inhibit electron flux through the protein in this manner.

We find that the efficiencies of the other altered proteins for N_2 reduction correlate well with the results of our modelling studies. Thus, the

Glu mutant is particularly poor for N_2 reduction, and we assign this to the electrostatic repulsion between the carboxylate group of the $-CH_2CH_2CO_2^-$ arm of homocitrate and the Glu side chain. The Asp mutant is also negatively charged but, in this case, the separation between the groups will be larger because of its shorter side chain and also because of the likely interaction between α-Asp426 and β-Arg100 discussed above. Hence the Glu altered protein is a significantly poorer N_2 fixer than the Asp-altered protein. After Glu, the Tyr and Arg-altered proteins are the next poorest for N_2 fixation. Both of these have the opposite H-bonding pattern to that of the wild type α-Lys426 residue; namely, an H-bond between the mutant side chain in the resting state but not in the ring-opened state. In addition, the bulky Tyr side chain is likely to hinder the motion of the homocitrate upon ring opening. Hence, the equilibrium between the ring-opened, N_2-binding state and the ring-closed state will be shifted in favour of the latter, making the Tyr and Arg variants relatively poor N_2 fixers. The observation that the α-Arg426 altered protein is similar to the wild type protein with respect to the efficiency of FeMoco insertion, and yet is a relatively poor N_2 fixer, strongly supports the contention that residue α-426 has a wider role than simply facilitating insertion of the FeMoco. The Met, Ala, His and Thr substitutions are all fairly neutral in that there are no specific interactions between their side chains and homocitrate. They are all slightly inferior in their N_2-fixing activity to the wild type because they lack the positive effect of Lys in promoting the interaction between homocitrate and α-His442.

Finally, the Gln mutant is of particular interest in that it shows a moderate, and yet reproducible, enhancement in N_2-reduction efficiency over the wild type protein. Our modelling studies indicate that this is the only other residue capable of forming an H-bond to homocitrate in its ring-opened, Mo-activating conformation (Figure 8). These experimental and theoretical results indicate that it may indeed be possible to construct better nitrogenases than wild type, provided the gain in functional efficiency is not offset by a loss in efficiency of cofactor insertion.

The α-Arg426 altered protein, like the *ΔnifV* altered protein, shows inhibition of H_2 evolution (i.e., uncoupling of ATP hydrolysis from electron transfer) in the presence of CO. In the active homocitrate model for H_2

evolution [25], this behaviour in the *ΔnifV* protein is explained in terms of a perturbation by CO of an equilibrium between a ring-opened MoH species A, which can rapidly evolve H_2, and a ring-closed species B, which is unreactive (Scheme 1). This scheme readily adapts to the α-Arg426 altered protein; the extra H-bonds between the Arg residue and the $-CH_2CH_2CO_2^-$ homocitrate arm that we observe in our model of the resting state of this altered protein would also help to stabilise B over A.

Sequence comparisons

The differences in amino acid sequence in the vicinity of the homocitrate ligand for the VFe-protein compared to the MoFe-protein (Table 3) are interesting in terms of potential H-bonds between these residues and homocitrate. The MoFe-protein X-ray crystal structures show a H-bond between the homocitrate $-CH_2CH_2CO_2^-$ arm and the backbone NH group of α-Ile425, which must be broken if the homocitrate undergoes chelate ring opening. The substitution of Ile by Pro in the VnfD sequences means that there is no possibility of an analogous interaction in VFe-proteins; indeed, the steric constraints of the Pro side chain would demand a different conformation for the $-CH_2CH_2CO_2^-$ group in the resting state. As we have seen, replacing α-Lys426 by Arg in the MoFe-protein reduces the efficiency of N_2 fixation, because Arg can H-bond to homocitrate in the ring-closed but not the ring-opened conformation, the reverse pattern to the wild type Lys. However, in the case of the VFe-proteins, the substitution of Ile for Pro, together with the other local sequence changes, especially in the three residues following α-Lys426, might be sufficient to switch this behaviour so that Arg becomes the preferred residue for interaction with homocitrate in the ring-opened state.

Further insight into this question can be gained by consideration of two hybrid proteins, namely the VFe component 1 protein complemented with FeMoco [44], and the MoFe-protein complemented with FeVco [45]. Whereas the VFe-protein/FeMoco combination behaves like normal MoFe-protein with respect to N_2 reduction, the MoFe-protein/FeVco combination does not reduce N_2 at all. If the homocitrate chelate ring opening is intrinsically more difficult for FeVco than for FeMoco, then the differences in the protein sequences may reflect a compensating promotion of the ring-opened state by the protein environment for the VFe-protein.

Finally, we note that α-Gly424 is strictly conserved across all the MoFe and VFe-protein sequences. Modelling the effects of substituting this residue by Ala, we find that there would be a steric clash between homocitrate and α-Ala424 in both the ring-closed and -opened homocitrate conformations. Given that replacement of α-Ile425 by Pro in the VFe-protein sequences must produce a similar steric clash in the resting state, and yet the VFe-protein/FeMoco hybrid is viable for N_2 reduction, it seems unlikely that the α-Ala424 mutation would be a serious problem for the ring-closed state. However, modelling the α-Ala424 ring-opened state suggests that this mutation would prevent the interaction between homocitrate and α-His442, possibly producing similar phenotypes to those we observe for the α-Lys426 mutants.

In summary, we have proposed that the α-Lys426 residue anchors homocitrate so it can H-bond to α-His442, which helps optimize N_2 reduction, and we have shown that disrupting the α-Lys426 H-bond to homocitrate compromises N_2 reduction. α-Lys426 is more than twice the distance from the Fe-S face of FeMoco adjacent to α-Val70 than is Mo. Thus, we find it even more difficult to understand how the mutations at α-Lys426 could affect N_2 binding and reduction if this occurred at the α-Val70 site, than do Barney *et al*. [12] to imagine how Mo could participate in N_2 binding because of the effects of mutations at α-Val70. Further experiments are clearly necessary to resolve these apparent inconsistencies. Although there is a growing body of evidence that supports alkynes and alkenes being bound and reduced at or close to the α-Val70 Fe-S face of FeMoco, our results support Mo as the favoured binding and reduction site for N_2.

Acknowledgment: Financial support of the Biotechnology and Biological Sciences Research Council (a postdoctoral award to KF) and the Competitive Strategic Grant to the JIC is gratefully acknowledged. We thank Dr Shirley Fairhurst for help with the EPR measurements. WEN thanks the NIH (DK-37255) for support.

References

1. Burgess, B.K. and Lowe, D.J. (1996) Mechanism of molybdenum nitrogenase. Chem. Rev. **96**, 2983-3012.

2. Chan, M.K., Kim, J. and Rees, D.C. (1993) The nitrogenase FeMo-cofactor and P-cluster pair: 2.2Å resolution structures. Science **260**, 792-794.

3. Einsle O., Tezcan, F.A., Andrade S.L., Schmid B., Yoshida M., Howard J.B., and Rees D.C. (2002) Nitrogenase MoFe-protein at 1.16 Å resolution: a central ligand in the FeMo-cofactor. Science **297**, 1654-5.

4. Lee, H.I., Thrasher, K.S., Dean, D.R., Newton, W.E. and Hoffman, B.M. (1998) ^{14}N Electron Spin-Echo Envelope Modulation of the $S = {}^{3}/_{2}$ Spin System of the *Azotobacter vinelandii* Nitrogenase Iron-Molybdenum Cofactor Biochemistry **37**, 13370-13378.

5. Thorneley R.N.F and Lowe, D.J. (1984) The mechanism of *Klebsiella pneumoniae* nitrogenase action. Simulation of the dependences of H_2-evolution rate on component-protein concentration and ratio and sodium dithionite concentration. Biochem. J. **224**, 903-909.

6. Georgiadis, M. M.; Komiya, H.; Chakrabarti, P.; Woo, D.; Kornuc, J. J.; Rees, D. C. (1992) Crystallographic structure of the nitrogenase iron protein from Azotobacter vinelandii Science, **257**, 1653-9.

7. Kim, J.; Rees, D. C. (1992) Structural models for the metal centers in the nitrogenase molybdenum-iron protein Science, **257**, 1677-82.

8. Schindelin, H.; Kisker C.; Schlessman, J. L.; Howard, J. B.; Rees, D. C. (1997) Structure of ADP x AIF4(-)-stabilized nitrogenase complex and its implications for signal transduction, Nature **387**, 370-76.

9. Mayer, S. M., Lawson, D. M., Gormal, C. A., Roe, S. M., and Smith, B. E. (1999) New insights into structure-function relationships in nitrogenase: a 1.6 Å resolution X-ray crystallographic study of *Klebsiella pneumoniae* MoFe-protein. J. Mol. Biol. **292**, 871-891.

10. Dos Santos, P.C., Igarashi, R.Y., Lee, H.I., Hoffman, B.M., Seefeldt, L.C. and Dean, D.R. (2005) Substrate Interactions with the Nitrogenase Active Site. Acc. Chem. Res, **38**, 208 – 214.

11. Barney, B.M., Laryukhin, M., Igarashi, R.Y., Lee., H.I., Dos Santos, P.C., Yang, T-C, Hoffman, B.M., Dean, D.R., and Seefeldt, L.C (2005) Trapping a hydrazine intermediate on the nitrogenase active site. Biochemistry **44**, 8030-8037.

12. Barney B.M., Yang, T-C, Igarashi, R.Y., Dos Santos, P.C., Laryukhin, M., Lee, H.I., Hoffman, B.M., Dean, D.R., and Seefeldt, L.C. (2005) Intermediates trapped during nitrogenase reduction of N≡N, CH_3-N=NH, and H_2N-NH_2. J. Am. Chem. Soc. **127**:14960-14961.

13. Durrant, M. C. (2002) An atomic level mechanism for molybdenum nitrogenase. Part 1. Reduction of dinitrogen. Biochemistry **41**, 13934-13945.

14. Kastner, J., Hemmen, S., Blochl, P.E. (2005)**.** Activation and protonation of dinitrogen at the FeMo cofactor of nitrogenase. J Chem Phys. **123**, 74306.

15. Huniar, U., Ahlrichs, R. and Coucouvanis, D. (2004) Density functional theory calculations and exploration of a possible mechanism of N_2 reduction by nitrogenase. J. Am. Chem. Soc. **126**, 2588-601.

16. Dance, I. (2004) The mechanism of nitrogenase. Computed details of the site and geometry of binding of alkyne and alkene substrates and intermediates. J Am Chem Soc.**126**, 11852-63.

17. Dance, I. (2005) The hydrogen chemistry of the FeMo-co active site of nitrogenase. J Am Chem Soc.**127**, 10925-42.

18. Durrant, M. C. (2004) An atomic level model for the interactions of molybdenum nitrogenase with carbon monoxide, acetylene, and ethylene. Biochemistry **43**, 6030-6042.

19. Hawkes, T. R., McLean, P. A. and Smith, B. E. (1984) Nitrogenase from nifV mutants of *Klebsiella pneumoniae* contains an altered form of the iron-molybdenum cofactor. Biochem J. **217**, 317–321.

20. Newton, W. E. Vichitphan, K. and Fisher, K. (2002) Substrate reduction and CO susceptibility of the ΔNifV and α-Q191K MoFe-proteins of Azotobacter vinelandii nitrogenase.In Nitrogen Fixation: Global Perspectives (T. Finan, M. R. O'Brian, D. B. Layzell, J. K. Vessey and W. E. Newton, eds.) CABI Publishing, NY, p. 370.

21. Imperial, J., Hoover, T. R., Madden, M. S., Ludden, P. W., and Shah, V. K. (1989) Substrate reduction properties of dinitrogenase activated *in vitro* are dependent upon the presence of homocitrate or its analogues during iron-molybdenum cofactor synthesis. Biochemistry **28**, 7796-9.

22. Pickett, C. J. (1996) The Chatt Cycle and the Mechanism of Enzymic Reduction of Molecular Nitrogen. J Biological Inorganic Chemistry, **1** 601-606.

23. Grönberg, K. L., Gormal, C. A., Durrant, M. C., Smith, B. E. and Henderson, R.A. (1998) Why R-Homocitrate is essential to the reactivity of FeMo-cofactor of nitrogenase: studies on $NifV^-$ extracted FeMo-cofactor. J. Amer. Chem. Soc., **120**, 10613-10621.

24. Durrant M. C. (2001) Controlled protonation of iron-molybdenum cofactor by nitrogenase: a structural and theoretical analysis. Biochem J. **355**, 569-76.

25. Durrant, M. C. (2002) An atomic-level mechanism for molybdenum nitrogenase. Part 2. Proton reduction, inhibition of dinitrogen reduction by dihydrogen, and the HD formation reaction. Biochemistry **41**, 13946-55.

26. Hales, B. J. and Case, E. E. (1987) Nitrogen fixation by Azotobacter vinelandii in tungsten-containing medium. J. Biol. Chem. **262**, 16205-11.

27. Ho, S .N., Hunt, H. D., Horton, R. M., Pullen, J. K. and Pease, L. R. (1989) Site-Directed Mutagenesis by Overlap extension using the polymerase chain reaction. Gene **77**, 51-59

28. Shen, J., Dean, D. R. and Newton, W. E. (1997) Evidence for multiple substrate-reduction sites and distinct inhibitor-binding sites from an altered *Azotobacter vinelandii* nitrogenase MoFe-protein. Biochemistry, **36**, 4884 – 4894.

29. Strandberg, G. W. and Wilson, P. W. (1968) Formation of the nitrogen-fixing enzyme system in Azotobacter vinelandii. Canadian Journal of Microbiology, **14**, 25-32.

30. Kim, C-H., Newton, W. E. and Dean, D. R. (1995) Role of the MoFe-protein alpha.-subunit histidine-195 residue in FeMo-cofactor binding and nitrogenase catalysis. Biochemistry; **34**, 2798 – 2808.

31. Dilworth, M. J., Eldridge, M. E. and Eady, R. R. (1992. Correction for creatine interference with the direct indophenol measurement of NH_3 in steady-state nitrogenase assays. Anal. Biochem. **207**, 6-10.

32. Dilworth, M. J. and Fisher, K. (1998) Elimination of creatine interference with the indophenol measurement of NH_3 produced during nitrogenase assays. Anal. Biochem. **256**, 242-4.

33. Lowry, O. H., Rosebrough, N. J., Farr, A. L. and Randall, R. J. (1951) Protein measurement with the Folin phenol reagent. J. Biol. Chem. **193**, 265–275.

34. Fisher, K., Newton, W. E. and Lowe, D. J. (2001) Electron Paramagnetic Resonance Analysis of Different *Azotobacter vinelandii* Nitrogenase MoFe-Protein Conformations during Enzyme Turnover: Evidence for *S* = 3/2 Spin States from Reduced MoFe-Protein Intermediates. Biochem. J. **40**, 3333-3339.

35. Laemmli, U. K. (1970) Cleavage of structural proteins during the assembly of the head of bacteriophage T4.Nature. **227**, 680-5.

36. Insight II, version 2000.1 (2000), Accelrys Ltd., Cambridge CB4 0WN, UK.

37. Berman, H. M., Westbrook, J., Feng, Z., Gilliland, G., Bhat, T. N., Weissig, H., Shindyalov, I. N, and Bourne, P. E. (2000) The Protein Data Bank. Nucleic Acids Research **28**, 235-242.

38. Maskos, Z., Fisher, K., Sorlie, M., Newton, W. E. and Hales, B. J. (2005) Variant MoFe-proteins of Azotobacter vinelandii: effects of

carbon monoxide on electron paramagnetic resonance spectra generated during enzyme turnover. J Biol Inorg Chem. **10**, 394-406.

39. Hwang, J. C. and Burris R. H. (1972) Nitrogenase-catalyzed reactions. Biochim Biophys Acta. **283**, 339-50.

40. Edgar, R. C. (2004). MUSCLE: multiple sequence alignment with high accuracy and high throughput, Nucleic Acids Res. **32**, 1792-1797.

41. Scott, D. J., Dean, D. R. and Newton, W. E. (1992) Nitrogenase catalysed ethane production and CO-sensitive hydrogen evolution from MoFe-proteins having amino acid substitutions in an alpha-subunit FeMo cofactor-binding domain. J. Biol. Chem. **267**, 20002-10.

42. Dos Santos, P. C., Dean, D. R., Hu, Y., and Ribbe, M. W. (2004) Formation and insertion of the nitrogenase iron-molybdenum Cofactor. Chem. Rev. **104**, 1159-1173.

43. Christiansen, J., Cash, V. L., Seefeldt, L. C. and Dean, D. R. (2000) Isolation and characterization of an acetylene-resistant nitrogenase. J Biol Chem. **275**, 11459-64.

44. Moore, V. G., Tittsworth, R. C., and Hales, B. J. (1994). Construction and characterization of hybrid component 1 from V-nitrogenase containing FeMo cofactor. J. Am. Chem. Soc. **116**, 12101-12102.

45. Smith, B. E., Eady, R. R., Lowe, D. J., and Gormal, C. A.(1988) The vanadium-iron protein of vanadium nitrogenase from *Azotobacter croococcum* contains an iron-vanadium cofactor. Biochem. J. **250**, 299-302.

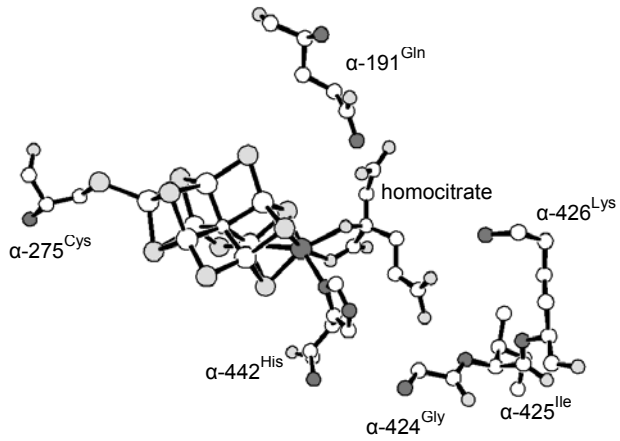

Figure1

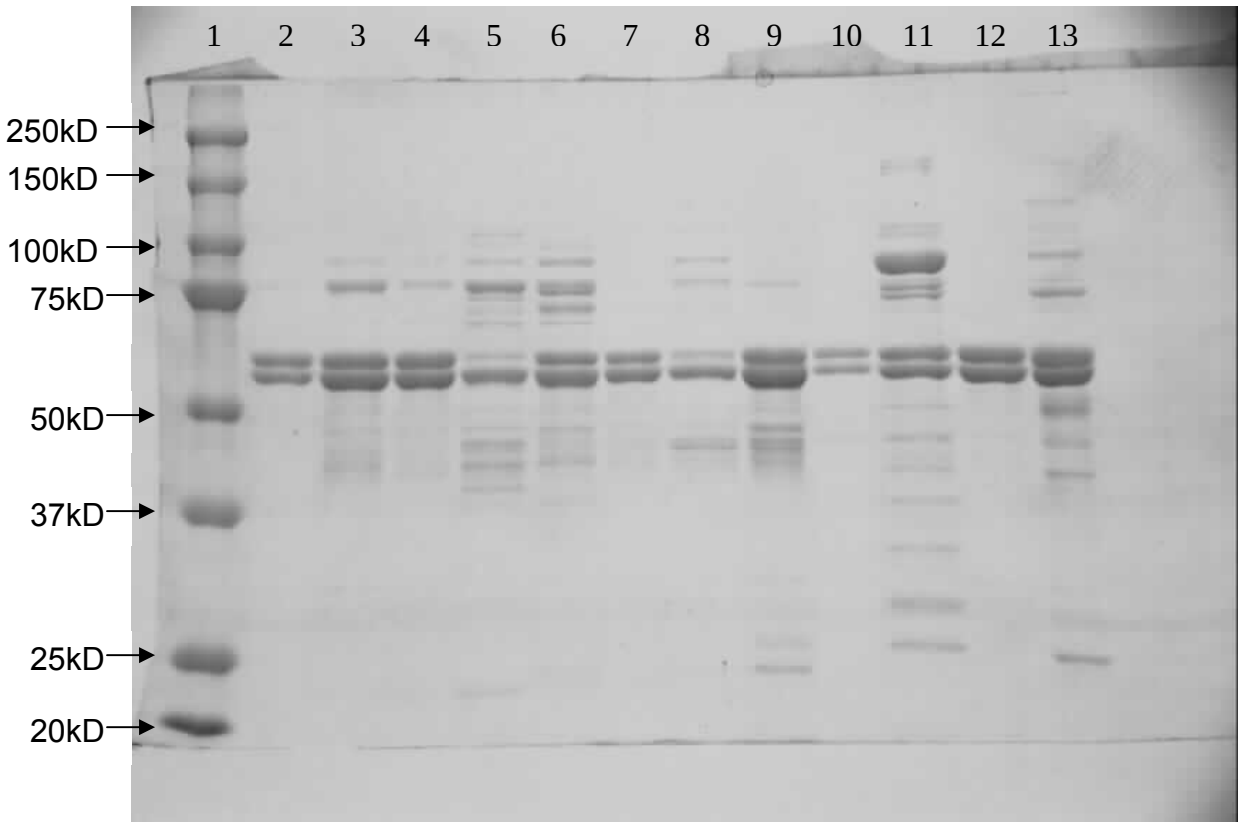

Figure 2

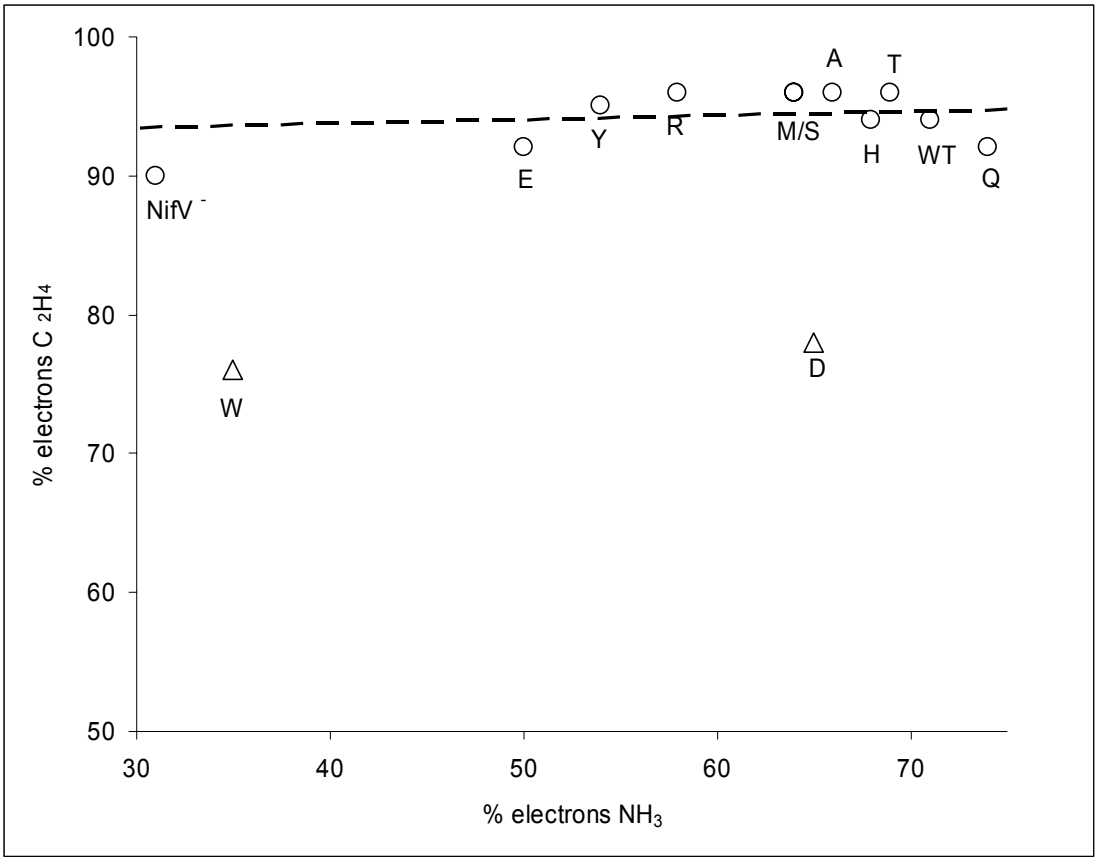

Figure 3

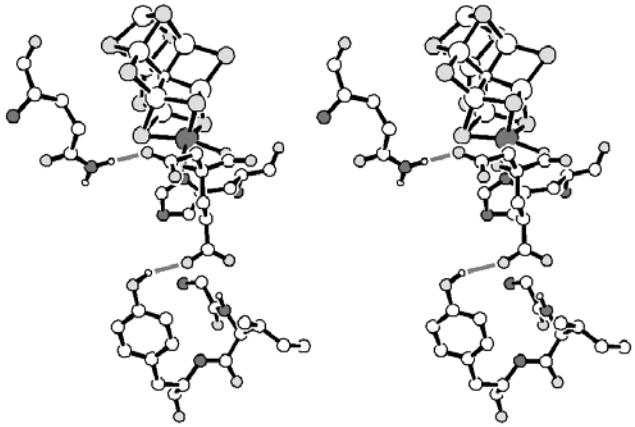

Figure 4

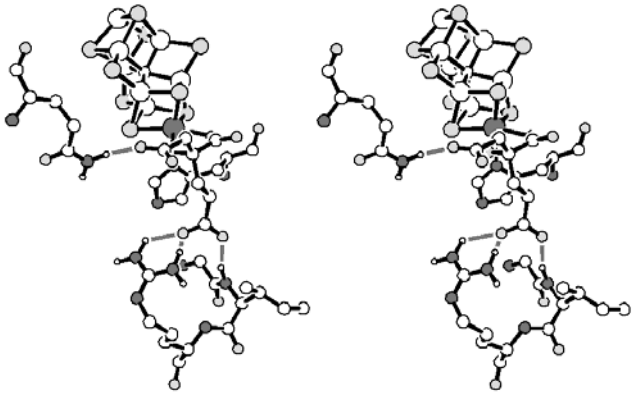

Figure 5

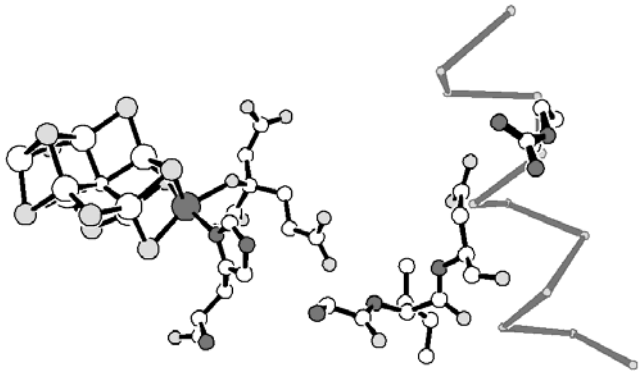

Figure 6 (Asp variant)

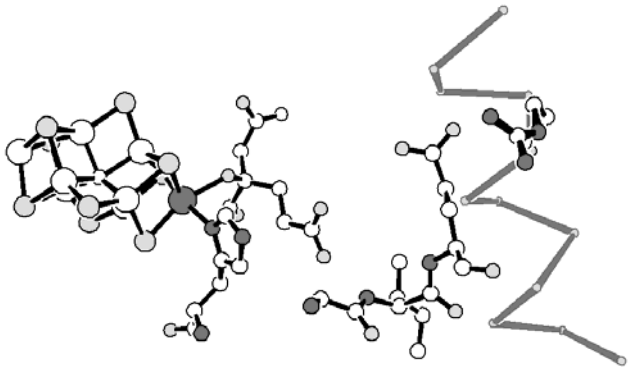

Figure 7. (Glu variant)

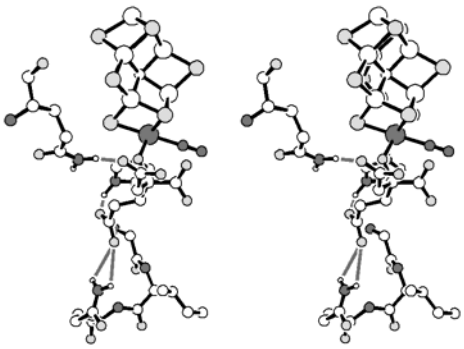

Figure 8. (note the dinitrogen ligand on Mo; for clarity, only the imidazole ring of His442 is shown)

Biochemical Journal Immediate Publication. Published on 27 Mar 2006 as manuscript BJ20060102

Table 1: Diazotrophic growth and purification properties of wild-type and α-426 altered MoFe-proteins.

MoFe-protein	Doubling time (hr)	CE SPA	Purified MoFe-protein SPA	[Mo]	[Fe]:[Mo]	% WT g=3.7 EPR Intensity
WT	3.5	150	2500	1.6	16	100
α-426A	4.1	108	1300	1.0	28	60
α-426T	4.5	105	1400	1.3	15	70
α-426Q	4.5	64	1940	1.8	15	91
α-426S	4.7	89	1300	1.2	16	60
α-426R	5.6	101	2500	1.5	12	100
α-426H	5.6	37	340	0.6	15	20
α-426M	5.8	56	850	0.5	28	40
α-426Y	7.9	65	650	0.8	35	30
α-426E	8.9	34	200	0.2	67	10
α-426D	11.8	12	320	0.7	64	10
α-426W	12.8	55	170	0.3	80	10

All SPA values are nmol H_2 $(min.mg)^{-1}$ with an excess of Fe-protein.

Table 2: Substrate binding affinities and ATP:2e data for wild type and α-426 altered MoFe-proteins under 10% C_2H_2 /90% Ar and100% N_2.

MoFe-protein	% total e- to C_2H_4	ATP:2e C_2H_2	K_m C_2H_2 (Kpa)	% total e- to NH_3	ATP:2e N_2	K_m N_2 (KPa)
WT	94	4.7	0.83 ±0.03	71	6.1	8.2 ± 0.6
α-426A	96	6.1	0.51 ±0.02	66	7.6	9.4 ± 1.7
α-426T	96	6.6	0.49 ±0.03	69	7.2	7.5 ± 0.3
α-426Q	92	6.2	0.64 ± 0.05	74	6.0	9.2 ± 04
α-426S	96	6.1	0.49 ± 0.02	64	6.6	7.5 ± 0.3
α-426R	96	5.2	0.9 ± 0.05	58	5.8	24.2 ± 3.8
α-426H	94	6.8	0.52 ± 0.03	68	6.8	9.0 ± 1.0
α-426M	96	6.6	0.61 ± 0.02	64	6.6	10.3 ± 0.6
α-426Y	95	13.5	0.53 ±0.03	54	11.2	11.7 ± 1.1
α-426E	92	20.4	0.43 ± 0.02	50	14.6	9.6 ± 1.0
α-426D	78	29.7	0.31 ±0.04	65	10.8	7.3 ± 0.6
α-426W	75	32.3	0.61 ± 0.03	35	20.6	15.4 ± 3.1
ΔNifV	90	nd	nd	31	nd	nd

Biochemical Journal Immediate Publication. Published on 27 Mar 2006 as manuscript BJ20060102

Table 3. Amino acid sequence analysis for MoFe and VFe α-chain sequences, residues 421 – 429[1].

MoFe-protein sequences								
Val (34)	**Gly** (29)	**Ser** (57)	**Gly** (68)	**Ile** (50)	**Lys**[2] (68)	**Glu** (61)	**Lys** (67)	**Tyr** (66)
Ile (19)	**Ala** (26)	**Ala** (9)		**Val** (17)		**Asp** (7)	**Arg** (1)	**Phe** (2)
Phe (8)	**Cys** (5)	**Val** (1)		**Leu** (1)				
Met (7)	**Phe** (4)	**Gly** (1)						
	Leu (4)							
VFe-protein sequences								
Ile (5)	**Phe** (5)	**Thr** (6)	**Gly** (6)	**Pro** (6)	**Arg** (6)	**Val** (6)	**Gly** (6)	**Glu** (3)
Val (1)	**Leu** (1)							**Asp** (2)
								Ala (1)

[1]Numbering taken from Av1 sequence. Figures in parentheses are the number of sequences incorporating each residue.

[2]One MoFe-protein sequence has an extra Glu inserted between residues 426 and 427.

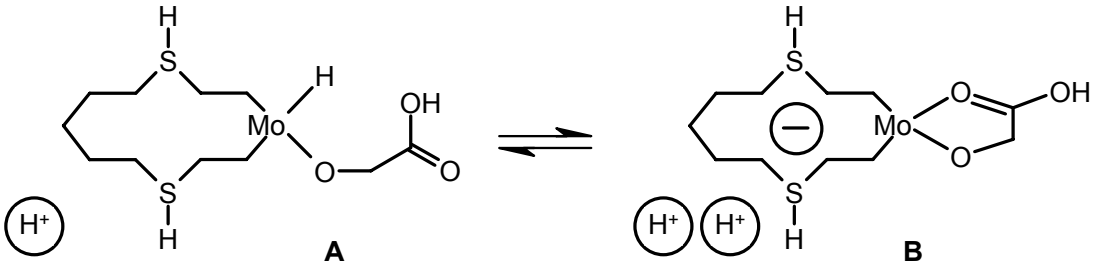

Scheme 1. Proposed equilibrium at Lowe-Thorneley redox state E_4 between a Mo hydride, **A**, which evolves H_2 rapidly by hydrolysis, and a relatively stable, homocitrate ring-closed species **B**, as described in Durrant [25]. H^+ in circles denote protons attached to amino acid side chains in the vicinity of FeMoco. Note that the charge on FeMoco is increased by one electron relative to the original model [18].

Figure captions

Figure 1. Iron-molybdenum cofactor and selected residues of importance in this study. This and other structure figures drawn using ORTEP-3 for windows, version 1.08 [Farrugia, L.J. (1997) J. App. Cryst., **30**, 565]. Atomic coordinates taken from X-ray crystal structure 1M1N (ref. 4). Atoms shaded as follows: dark grey, Mo and N; light grey, S and O; white, Fe and C.

Figure 2. 10% SDS-PAGE of MoFe-proteins purified from the α-426 mutant strains and wild type. Lane 1: Molecular weight marker (250, 150, 100, 75, 50, 37, 25, 20 kDa); Lane 2: wild type MoFe-protein; Lane 3: α-Ser426 MoFe-protein; Lane 4: α-Thr426 MoFe-protein; Lane 5: α-Glu426 MoFe-protein; Lane 6: α-Met426 MoFe-protein; Lane 7: α-Ala426 MoFe-protein; Lane 8: α-Trp426 MoFe-protein; Lane 9: α-Tyr426 MoFe-protein; Lane 10: α-Arg426 MoFe-protein; Lane 11: α-His426 MoFe-protein; Lane 12: α-Gln426 MoFe-protein and Lane 13: α-Asp426 MoFe-protein. Lanes 2-13 contain approximately 0.2μg MoFe-protein.

Figure 3. Comparison of electron distribution to NH_3 and C_2H_4 during N_2 and C_2H_2 reduction by wild type, ΔNifV and altered α-426 MoFe-proteins. Assays contained 10% C_2H_2:90% Ar or 100% N_2 and were initiated with a 20:1 mix of Av2:Av1. Assays were run for 40 min and were quenched with 0.3mL 0.5M EDTA pH7.5. Linearity was checked by quenching assays at 16 min (data not shown). Each assay contained 0.0375 mg MoFe-protein. Proteins are represented by the single amino acid letter code. The dashed line is a best fit to the points excluding the Trp(W) and Asp(D) data which do not fit this correlation.

Figure 4. Stereo view of the model of the resting form of the α-Tyr426 mutant. Atom shading as in Figure 1; selected H atoms and predicted H-bonds are shown as small circles and grey lines, respectively. Note the H-bonds between homocitrate and α-Gln191, as seen in the wild type structure,

and the phenolic OH group of α-Tyr426, formed at the expense of the H-bond to the α-Ile425 backbone NH group.

Figure 5. Stereo view of the model of the resting form of the α-Arg426 mutant. Atom shading as in Figure 1; selected H atoms and predicted H-bonds are shown as small circles and grey lines, respectively. In addition to the H-bonds between homocitrate and the α-Gln191 side chain, and the α-Ile425 backbone NH group, both of which are seen in the wild type structure, the α-Arg426 side chain has formed a bifurcating H-bond with homocitrate.

Figure 6. Model for the resting state of the α-Asp426 mutant. Atom shading as in Figure 1. The α-helix incorporating residues 96 – 107 of the β-subunit is shown in grey as an α-carbon trace, with the side chain of residue β-Arg100 included in ball and stick mode. Note the orientation of the Asp side chain towards the Arg side chain.

Figure 7. Model for the resting state of the α-Glu426 mutant. Shading and rendering as in Figure 6.

Figure 8. Model for the ring-opened state of the α-Gln426 mutant. Atom shading as in Figure 1; selected H atoms and predicted H-bonds are shown as small circles and grey lines, respectively. Note the N_2 ligand on Mo; for clarity, only the imidazole ring of α-His442 is shown. In addition to the usual H-bond between homocitrate and α-Gln191, there is a bifurcating H-bond between homocitrate and the α-Gln426 side chain, and the putative functionally significant H-bond between homocitrate and the imidazole NH group of α-His442.